Eur. Phys. J. C 46, 451–464 (2006)
Digital Object Identifier (DOI) 10.1140/epjc/s2006-02504-0

THE EUROPEAN PHYSICAL JOURNAL C

# Probing the QCD equation of state with thermal photons in nucleus–nucleus collisions at RHIC

D. d'Enterria[a], D. Peressounko[2]

[1] Nevis Laboratories, Columbia University, Irvington, NY 10533, and New York, NY 10027, USA
[2] RRC "Kurchatov Institute", Kurchatov Sq. 1, Moscow, 123182, Russia

Received: 7 October 2005 / Revised version: 29 December 2005 /
Published online: 30 March 2006 – 

**Abstract.** Thermal photon production at mid-rapidity in Au + Au reactions at $\sqrt{s_{\rm NN}} = 200$ GeV is studied in the framework of a hydrodynamical model that describes efficiently the bulk identified hadron spectra at RHIC. The combined thermal plus NLO pQCD photon spectrum is in good agreement with the yields measured by the PHENIX experiment for all Au + Au centralities. Within our model, we demonstrate that the correlation of the thermal photon slopes with the charged hadron multiplicity in each centrality provides direct empirical information on the underlying degrees of freedom and on the form of the equation of state, $s(T)/T^3$, of the strongly interacting matter produced in the course of the reaction.

**PACS.** 12.38.Mh; 24.10.Nz; 25.75.-q; 25.75.Nq

## 1 Introduction

Numerical calculations of lattice QCD predict a transition from ordinary hadronic matter to a deconfined state of quarks and gluons when the temperature of the system is of the order of $T_{\rm crit} \approx 0.17$ GeV [1].

The existence of such a phase transition manifests itself clearly in the QCD equation-of-state (EoS) on the lattice by a sharp jump of the (Stefan–Boltzmann) scaled energy density, $\varepsilon(T)/T^4$, at the critical temperature, reminiscent of a first-order phase change[1]. The search for evidence of this deconfined plasma of quarks and gluons (QGP) is the main driving force behind the study of relativistic nuclear collisions at different experimental facilities in the last 20 years. Whereas several experimental results have been found consistent with the formation of the QGP both at CERN-SPS [2] and BNL-RHIC [3] energies, it is fair to acknowledge that there is no incontrovertible proof yet of bulk deconfinement in the present nucleus–nucleus data. In this paper, we present a detailed study of the only experimental signature, thermal photons, that can likely provide direct information on the *thermodynamical* properties (and, thus, on the equation-of-state) of the underlying QCD matter produced in high-energy heavy-ion collisions. Electromagnetic radiation (real and virtual photons) emitted in the course of a heavy-ion reaction, has long [4, 5] been considered a privileged probe of the space-time evolution of the colliding system[2], in as much as photons are not distorted by final-state interactions due to their weak interaction with the surrounding medium. Direct photons, defined as real photons not originating from the decay of final hadrons, are emitted at various stages of the reaction with several contributing processes. Two generic mechanisms are usually considered: (i) *prompt* (pre-equilibrium or pQCD) photon emission from perturbative parton–parton scatterings in the first tenths of fm/$c$ of the collision process, (ii) subsequent $\gamma$ emission from the *thermalized* partonic (QGP) and hadronic (hadron resonance gas, HRG) phases of the reaction.

Experimentally, direct-$\gamma$ data have been indeed measured in Pb + Pb collisions at CERN-SPS ($\sqrt{s_{NN}} = 17.3$ GeV) [9]. However, the relative contributions to the total spectrum of the pQCD, QGP and HRG components have not been determined conclusively. Different hydrodynamics calculations [10–14] require "non-conventional" conditions: high initial temperatures ($T_0^{\rm max} > T_{\rm crit}$), strong partonic and/or hadronic transverse velocity flows, or in-medium modifications of hadron masses, in order to reproduce the observed photon spectrum. However, no final conclusion can be drawn from these results due mainly to the uncertainties in the exact amount of radiation coming from primary parton–parton collisions. In a situation akin to that affecting the interpretation of high $p_{\rm T}$ hadron data at SPS [15], the absence of a concurrent baseline experimental measurement of prompt photon production

[a] e-mail: denterria@nevis.columbia.edu

[1] The order of the phase transition itself is not exactly known: the pure SU(3) gauge theory is first-order whereas introduction of 2 + 1 flavours makes it of a fast cross-over type [1].

[2] Excellent reviews on photon production in relativistic nuclear collisions have been published recently [6–8].

in $p+p$ collisions at the same $\sqrt{s}$ and $p_{\rm T}$ range as the nucleus–nucleus data, makes it difficult to have any reliable empirical estimate of the actual thermal $\gamma$ excess in the Pb + Pb spectrum. In the theoretical side, the situation at SPS is not fully under control either: (i) next-to-leading-order (NLO) perturbative calculations are known to underpredict the experimental reference nucleon–nucleon $\gamma$ differential cross sections below $\sqrt{s} \approx 30$ GeV [16] (a substantial amount of parton intrinsic transverse momentum $k_{\rm T}$ [17], approximating the effects of parton Fermi motion and soft gluon radiation, is required [18]), (ii) the implementation of the extra nuclear $k_{\rm T}$ broadening observed in the nuclear data ("Cronin enhancement" [19] resulting from multiple soft and semi-hard interactions of the colliding partons on their way in/out of the traversed nucleus) is model-dependent [20–22] and introduces an additional uncertainty to the computation of the yields, and (iii) hydrodynamical calculations usually assume initial conditions (longitudinal boost invariance, short thermalization times, zero baryochemical potential) too idealistic for SPS energies. The situation at RHIC (and LHC) collider energies is undoubtedly far more advantageous. Firstly, the photon spectra for different centralities in Au + Au [23] and in (baseline) $p+p$ [24] collisions at $\sqrt{s} = 200$ GeV are already experimentally available. Secondly, the $p+p$ baseline reference is well under control theoretically (NLO calculations do not require extra non-perturbative effects to reproduce the hard spectra at RHIC [24, 25]). Thirdly, the amount of nuclear Cronin enhancement experimentally observed is very modest (high $p_{\rm T}$ $\pi^0$ are barely enhanced in $d+$Au collisions at $\sqrt{s_{NN}} = 200$ GeV [26]), and one expects even less enhancement for $\gamma$ which, once produced, do not gain any extra $k_{\rm T}$ in their way out through the nucleus. Last but not least, the produced system at midrapidity in heavy-ion reactions at RHIC top energies is much closer to the zero net baryon density and longitudinally boost-invariant conditions customarily presupposed in the determination of the parametrized photon rates and in the hydrodynamical implementations of the reaction evolution. In addition, the thermalization times usually assumed in the hydrodynamical models ($\tau_{\rm therm} \lesssim 1$ fm/$c$) are, for the first time at RHIC, above the lower limit imposed by the transit time of the two colliding nuclei ($\tau_0 = 2R/\gamma \approx 0.15$ fm/$c$ for Au + Au at 200 GeV). As a matter of fact, it is for the first time at RHIC that hydrodynamics predictions agree *quantitatively* with most of the differential observables of bulk ("soft") hadronic production below $p_{\rm T} \approx 1.5$ GeV/$c$ in Au + Au reactions [27–29].

In this context, the purpose of this paper is threefold. First of all, we present a relativistic Bjorken hydrodynamics model that reproduces well the identified hadron spectra measured at all centralities in Au + Au collisions at $\sqrt{s_{NN}} = 200$ GeV (and, thus, the centrality dependence of the total charged hadron multiplicity). Secondly, using such a model complemented with the most up-to-date parametrizations of the QGP and HRG photon emission rates, we determine the expected thermal photon yields in Au + Au reactions and compare them to the prompt photon yields computed in NLO perturbative QCD. The combined inclusive (thermal+pQCD) photon spectrum is successfully confronted to recent results from the PHENIX collaboration as well as to other available predictions. Thirdly, after discussing in which $p_{\rm T}$ range the thermal photon signal can be potentially identified experimentally, we address the issue of how to have access to the thermodynamical properties (temperature, entropy density) of the radiating matter. We propose the correlation of two experimentally measurable quantities: the thermal photon slope and the multiplicity of charged hadrons produced in the reaction, as a direct method to determine the underlying degrees of freedom and the equation of state, $s(T)/T^3$, of the dense and hot QCD medium produced in Au + Au collisions at RHIC energies.

## 2 Hydrodynamical model

### 2.1 Implementation

Hydrodynamical approaches of particle production in heavy-ion collisions assume *local* conservation of energy and momentum in the hot and dense strongly interacting matter produced in the course of the reaction and describe its evolution using the equations of motion of perfect (non-viscous) relativistic hydrodynamics. These equations are nothing but the conservation of

(i) the energy-momentum tensor: $\partial_\mu T^{\mu\nu} = 0$ with $T^{\mu\nu} = (\varepsilon + p)u^\mu u^\nu - p\, g^{\mu\nu}$ [where $\varepsilon$, $p$, and $u^\nu = (\gamma, \gamma v)$ are respectively the energy density, pressure, and collective flow 4-velocity fields, and $g^{\mu\nu}$=diag(1,-1,-1,-1) the metric tensor], and

(ii) the conserved currents in strong interactions: $\partial_\mu J_i^\mu = 0$, with $J_i^\mu = n_i u^\mu$ [where $n_i$ is the number density of the net baryon, electric charge, net strangeness, etc. currents].

These equations complemented with three input ingredients: (i) the initial conditions ($\varepsilon_0$ at time $\tau_0$), (ii) the equation-of-state of the system, $p(\varepsilon, n_i)$, relating the local thermodynamical quantities, and (iii) the freeze-out conditions, describing the transition from the hydrodynamics regime to the free streaming final particles, are able to reproduce most of the bulk hadronic observables measured in heavy-ion reactions at RHIC [27–29].

The particular hydrodynamics implementation used in this work is discussed in detail in [12]. We assume cylindrical symmetry in the transverse direction ($r$) and longitudinal ($z$) boost-invariant (Bjorken) expansion [30] which reduces the equations of motion to a one-dimensional problem but results in a loss of the dependence of the observables on longitudinal degrees of freedom. Our results, thus, are only relevant for particle production within a finite range around midrapidity[3]. The equation-of-

[3] The experimental $\pi^\pm$ and $K^\pm$ d$N$/d$y$ distributions at RHIC are Gaussians [31], as expected from perturbative QCD initial conditions [32]. Thus, although there is no Bjorken rapidity plateau, the widths of the distributions are quite broad, and within $|y| \lesssim 2$, deviations from boost invariance are not very large [32].

state used here describes a first order phase transition from a QGP to a HRG at $T_{\rm crit} = 165\,{\rm MeV}$ with latent heat[4] $\Delta\varepsilon \approx 1.4\,{\rm GeV/fm^3}$, very similar to that used in other works [27]. The QGP is modeled as an ideal gas of massless quarks ($N_{\rm f} = 2.5$ flavours) and gluons with total degeneracy $g_{\rm QGP} = (g_{\rm gluons} + 7/8\, g_{\rm quarks}) = 42.25$. The corresponding EoS, $p = 1/3\varepsilon - 4/3B$ ($B$ being the bag constant), has sound velocity $c_{\rm s}^2 = \partial p/\partial\varepsilon = 1/3$. The hadronic phase is modeled as a non-interacting gas of $\sim$ 400 known hadrons and hadronic resonances with masses below $2.5\,{\rm GeV}/c^2$. The inclusion of heavy hadrons leads to an equation of state significantly different from that of an ideal gas of massless pions: the velocity of sound in the HRG phase is $c_{\rm s}^2 \approx 0.15$, resulting in a relatively soft hadronic EoS as suggested by lattice calculations [33]; and the effective number of degrees of freedom at $T_c$ is $g_{\rm HRG} \approx 12$ (as given by $g_{\rm eff} = 45\,s/(2\pi^2\,T^3)$; see later). Both phases are connected via the standard Gibbs' condition of phase equilibrium, $p_{\rm QGP}(T_c) = p_{\rm HRG}(T_c)$, during the mixed phase. The external bag pressure, calculated to fulfill this condition at $T_c$, is $B \approx 0.38\,{\rm GeV/fm^3}$. The system of equations is solved with the MacCormack two-step (predictor–corrector) numerical scheme [34] with time and radius steps: $\delta t = 0.02\,{\rm fm}/c$ and $\delta r = 0.1\,{\rm fm}$ respectively.

Statistical model analyses of particle production in nucleus–nucleus reactions [35] provide a very good description of the measured particle ratios at RHIC assuming that all hadrons are emitted from a thermalized system reaching chemical equilibrium at a temperature $T_{\rm chem}$ with baryonic, strange and isospin chemical potentials $\mu_i$. In agreement with those observations, our specific hydrodynamical evolution reaches chemical freeze-out at $T_{\rm chem} = 150\,{\rm MeV}$ with $\mu_{\rm B} = 25\,{\rm MeV}$ (as given by the latest statistical fits to hadron ratios [36]), and has $\mu_{\rm S} = \mu_{\rm I} = 0$. For temperatures above $T_{\rm chem}$ we conserve baryonic, strange and charge currents, but not particle numbers, while for temperatures below $T_{\rm chem}$ we explicitly conserve particle numbers by introducing individual (temperature-dependent) chemical potentials for each hadron. The final differential hadron ${\rm d}N/{\rm d}p_{\rm T}$ spectra are produced via a standard Cooper–Frye ansatz [37] at the kinetic freeze-out temperature ($T_{\rm fo} = 120\,{\rm MeV}$) when the hydrodynamical equations lose their validity, i.e. when the microscopic length (the hadrons mean free path) is no longer small compared to the size of the system. Unstable resonances are then allowed to decay with their appropriate branching ratios [38]. Table 1 summarizes the most important parameters describing our hydrodynamic evolution. The only free parameters are the initial energy density $\varepsilon_0$ in the center of the reaction zone for head-on (impact parameter $b = 0\,{\rm fm}$) Au + Au collisions at the starting time $\tau_0$, and the temperature at freeze-out time, $T_{\rm fo}$.

[4] Although the lattice results seem to indicate that the transition is of a fast cross-over type, the predicted change of $\Delta\varepsilon \approx 0.8\,{\rm GeV/fm^3}$ in a narrow temperature interval of $\Delta T \approx 20\,{\rm MeV}$ [1] can be interpreted as the latent heat of the transition.

### 2.2 Initialization

We distribute the initial energy density within the reaction volume according to the geometrical Glauber[5] prescription proposed by Kolb et al. [40]. Such an ansatz ascribes 75% of the initial entropy production in a given centrality bin, $s_0(b)$, to soft processes (scaling with the transverse density of participant nucleons $N_{\rm part}(b)$) and the remaining 25% to hard processes (scaling with the density of point-like collisions, $N_{\rm coll}(b)$, proportional to the nuclear overlap function $T_{AA}(b)$):

$$s(b) = C(0.25N_{\rm part}(b) + 0.75N_{\rm coll}(b)), \qquad (1)$$

where $C$ is a normalization coefficient chosen so that we produce the correct particle multiplicity at $b = 0\,{\rm fm}$. For each impact parameter, we construct an azimuthally symmetric hydrodynamical source from the (azimuthally deformed) initial Glauber entropy distribution, by defining a coordinate origin in the middle point between the centers of the two colliding nuclei and averaging the entropy density over all azimuthal directions. We then transform $\varepsilon_0(b) \propto s_0(b)^{4/3}$. This method provides a very good description of the measured centrality dependence of the final charged hadron rapidity densities ${\rm d}N_{\rm ch}/{\rm d}\eta$ measured at RHIC as can be seen in Fig. 1. Note that in our implementation of this prescription, we explicitly added the contribution of the particle multiplicity coming from hard processes (i.e. from hadrons having $p_{\rm T} > 1\,{\rm GeV}/c$) obtained from the scaled pQCD calculations

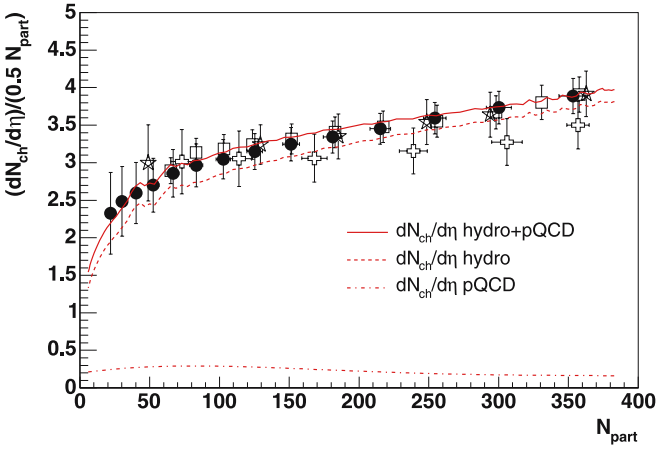


**Fig. 1.** Charged hadron multiplicity at midrapidity (normalized by the number of participant nucleon pairs) as a function of centrality (given by the number of participants, $N_{\rm part}$) measured in Au + Au at $\sqrt{s_{\rm NN}} = 200\,{\rm GeV}$ by PHENIX [41] (*circles*), STAR [42] (*stars*), PHOBOS [43] (*squares*) and BRAHMS [44] (*crosses*), compared to our hydrodynamics calculations (*dashed line*), our scaled pQCD ($p_{\rm T} > 1\,{\rm GeV}/c$) $p+p$ yields [45] (*dashed-dotted line*), and to the sum hydro+pQCD (*solid line*)

[5] The density of participant and colliding nucleons are obtained from the nuclear overlap function $T_{AA}(b)$ computed with a Glauber Monte Carlo code which parametrizes the Au nuclei with Woods–Saxon functions with radius $R = 6.38\,{\rm fm}$ and diffusivity $a = 0.54\,{\rm fm}$ [39].

**Table 1.** Summary of the thermodynamical parameters characterizing our hydrodynamical model evolution for central ($b = 0$ fm) Au + Au collisions at $\sqrt{s_{\rm NN}} = 200$ GeV. Input parameters are the (maximum) initial energy density $\varepsilon_0$ (with corresponding ideal-gas entropy densities $s_0$ and temperature $T_0$) at time $\tau_0$, the baryochemical potential $\mu_{\rm B}$, and the chemical and kinetic freeze-out temperatures $T_{\rm chem}$ and $T_{\rm fo}$ (or energy density $\varepsilon_{\rm fo}$). The energy densities at the end of the pure QGP ($\varepsilon^{\rm min}_{\rm QGP}$), and at the beginning of the pure hadron gas phase ($\varepsilon^{\rm max}_{\rm HRG}$) are also given for indication, as well as the average (over total volume) values of the initial energy density $\langle\varepsilon_0\rangle$, entropy density $\langle s_0\rangle$, and temperature $\langle T_0\rangle$

| $\tau_0$ (fm/$c$) | $\varepsilon_0$ ($\langle\varepsilon_0\rangle$) (GeV/fm$^3$) | $s_0(\langle s_0\rangle)$ (fm$^{-3}$) | $T_0$ ($\langle T_0\rangle$) (MeV) | $\varepsilon^{\rm min}_{\rm QGP}$ (GeV/fm$^3$) | $\varepsilon^{\rm max}_{\rm HRG}$ (GeV/fm$^3$) | $\mu_{\rm B}$ (MeV) | $T_{\rm chem}$ (MeV) | $T_{\rm fo}$ (MeV) | $\varepsilon_{\rm fo} = \varepsilon^{\rm min}_{\rm HRG}$ (GeV/fm$^3$) |
|---|---|---|---|---|---|---|---|---|---|
| 0.15 | 220 (72) | 498 (190) | 590 (378) | 1.7 | 0.35 | 25. | 150 | 120 | 0.10 |

(see later). Such a "perturbative" component accounts for a roughly constant $\sim 7\%$ factor of the total hadron multiplicity for all centralities. The good reproduction of the measured charged hadron integrated yields is an important result for our later use of $\mathrm{d}N_{\rm ch}/\mathrm{d}\eta|_{\eta=0}$ as an empirical measure of the initial entropy density in different Au + Au centrality classes (see Sect. 4).

For the initial conditions (Table 1), we choose $\varepsilon_0 = 220\,\mathrm{GeV/fm^3}$ (maximum energy density at $b = 0$ fm, corresponding to an *average* energy density over the total volume for head-on collisions of $\langle\varepsilon_0\rangle = 72\,\mathrm{GeV/fm^3}$) at a time $\tau_0 = 2R/\gamma \approx 0.15\,\mathrm{fm}/c$ equal to the transit time of the two Au nuclei at $\sqrt{s_{NN}} = 200$ GeV. The choice of this relatively short value of $\tau_0$ – otherwise typically considered in other hydrodynamical studies of thermal photon production at RHIC [10, 14, 46] – rather than the "standard" thermalization time of $\tau_{\rm therm} = 0.6\,\mathrm{fm}/c$ [27–29], is driven by our will to consistently take into account within our space-time evolution the emission of photons from secondary "cascading" parton–parton collisions [47, 48] taking place in the *thermalizing* phase between prompt pQCD emission (at $\tau \sim 1/p_{\rm T} \lesssim 0.15\,\mathrm{fm}/c$) and full equilibration (see Sect. 3.3). Though it may be questionable to identify such photons from second-chance parton–parton collisions as genuine *thermal* $\gamma$, it is clear that their spectrum reflects the momentum distribution of the partons during this thermalizing phase[6]. Additionally, recent theoretical works [49, 50] do seem to support the application of hydrodynamics equations in such "pre-thermalization" conditions. Our consequent space-time evolution leads to a value of the energy density of $\varepsilon \approx 30\,\mathrm{GeV/fm^3}$ at $\tau_{\rm therm} = 0.6\,\mathrm{fm}/c$, in perfect agreement with other 2D+1 hydrodynamic calculations which do not invoke azimuthal symmetry [27, 28] as well as more numerically involved 3D+1 approaches [29]. Thus, our calculations reproduce the final hadron spectra as well, at least, as those other works do. As a matter of fact, by using $\tau_0 = 0.15\,\mathrm{fm}/c$ (rather than $0.6\,\mathrm{fm}/c$), the system has a few more tenths of fm/$c$ to develop some extra transverse collective flow and there is no need to consider in our initial conditions a supplemental input radial flow velocity parameter, $v_{\rm r_0}$, as done in other works [12, 51] in order to reproduce the hadron spectra.

[6] Note also that it is precisely those secondary partonic interactions that are actually driving the system towards (local) thermal equilibrium.

### 2.3 Comparison to hadron data

Figure 2 shows the pion, kaon, and proton[7] transverse spectra measured by PHENIX [52], STAR [53, 54], PHOBOS [55] and BRAHMS [31] in central (0%–10% corresponding to $\langle b\rangle = 2.3$ fm) and peripheral (60%–70% corresponding to $\langle b\rangle = 11.9$ fm) Au + Au collisions at $\sqrt{s_{NN}} = 200$ GeV, compared to our hydrodynamical predictions (dashed lines) and to properly scaled $p+p$ NLO pQCD expectations [45] (dotted lines). At low transverse momentum, the agreement data–hydro is excellent starting from the very low $p_{\rm T}$ PHOBOS data ($p_{\rm T} < 100$ MeV) up to at least $p_{\rm T} \approx 1.5\,\mathrm{GeV}/c$. Above this value, contributions from perturbative processes (parton fragmentation products) start to dominate over bulk hydrodynamic production. Indeed, particles with transverse momenta $p_{\rm T} \gtrsim 2\,\mathrm{GeV}/c$ are mostly produced in primary parton–parton collisions at times of order $\tau \sim 1/p_{\rm T} \lesssim 0.15\,\mathrm{fm}/c$ (i.e. during the interpenetration of the colliding nuclei and *before* any sensible time estimate for equilibration), and as such, they are *not* in thermal equilibrium with the bulk particle production. Therefore, one does not expect hydrodynamics to reproduce the spectral shapes beyond $p_{\rm T} \approx 2\,\mathrm{GeV}/c$. The dotted lines of Fig. 2 show NLO predictions for $\pi$, $K$ and $p$ production in $p+p$ collisions at $\sqrt{s} = 200$ GeV [45] scaled by the number of point-like collisions ($N_{\rm coll} \propto T_{AA}$) times an empirical quenching factor, $R_{AA} = 0.2\,(0.7)$ for 0%–10% central (60%–70% peripheral) Au + Au, to account for the observed constant suppression factor of hadron yields at high $p_{\rm T}$ [56, 57] (such a suppression is not actually observed in the $p, \bar{p}$ spectra at intermediate $p_{\rm T} \approx 3$–$5\,\mathrm{GeV}/c$, see discussion below).

Figure 3 shows more clearly (in linear rather than log scale as the previous figure) the relative agreement between the experimental hadron transverse spectra and the hydrodynamical plus (quenched) pQCD yields presented in this work. The data-over-theory ratio plotted in the figure is obtained by taking the quotient of the pion, kaon and proton data measured in central Au + Au reactions (shown in the left plot of Fig. 2) over the corresponding sum of hydrodynamical plus perturbative results (solid lines in

[7] For a suitable comparison to the (feed-down corrected) PHENIX [52], PHOBOS [55] and BRAHMS [31] yields, the STAR proton spectra [53] have been appropriately corrected for a $\sim 40\%$ ($p_{\rm T}$-independent) contribution from weak decays [54].

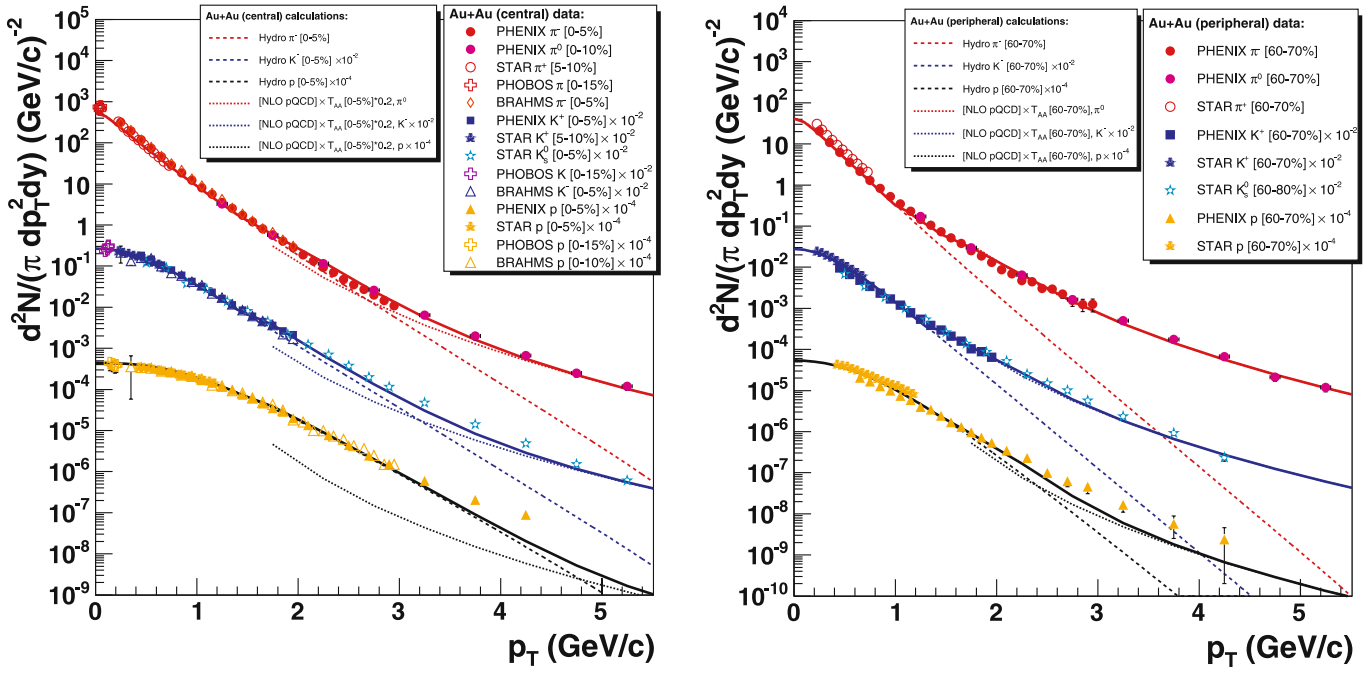


**Fig. 2.** Transverse momentum spectra for $\pi^{\pm,0}, K^{\pm,0}$, and protons measured in the range $p_{\rm T} = 0$–$5.5\,{\rm GeV}/c$ by PHENIX [52], STAR ($K^0_{\rm s}$ are preliminary) [53, 54], PHOBOS [55] and BRAHMS [31] in central (0%–10% centrality, *left*) and peripheral (60%–70%, *right*) Au + Au collisions at $\sqrt{s_{\rm NN}} = 200\,{\rm GeV}$, compared to our hydrodynamics calculations (*dashed lines*), to the scaled pQCD $p+p$ rates [45] (*dotted lines*), and to the sum hydro+pQCD (*solid lines*)

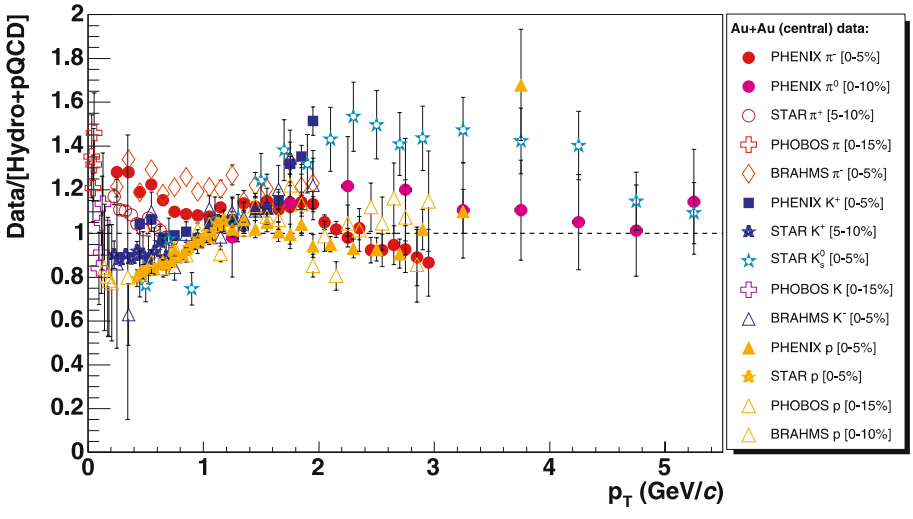


**Fig. 3.** Ratio of $\pi^{\pm,0}, K^{\pm,0}$, and proton yields measured in the range $p_{\rm T} = 0$–$5.5\,{\rm GeV}/c$ by PHENIX [52], STAR (note that $K^0_{\rm s}$ are preliminary) [53, 54], PHOBOS [55] and BRAHMS [31] in 0%–10% most central Au + Au collisions at $\sqrt{s_{\rm NN}} = 200\,{\rm GeV}$, over the sum hydro ($\langle b \rangle = 2.3\,{\rm fm}$) plus (quenched) pQCD. Theoretical calculations above $p_{\rm T} \approx 2\,{\rm GeV}/c$ have an overall ±20% uncertainty (not shown) dominated by pQCD scale uncertainties

Fig. 2). In the low $p_{\rm T}$ range dominated by hydrodynamical production, there exist some local $p_{\rm T}$-dependent deviations between the measurements and the calculations. However, the same is true within the independent data sets themselves and, thus, those differences are indicative of the amount of systematic uncertainties associated with the different measurements. High $p_{\rm T}$ hadro-production, dominated by perturbative processes, agrees also well within the $\sim 20\%$ errors associated with the standard scale uncertainties for pQCD calculations at this center-of-mass energy.

It is, thus, clear from Figs. 2 and 3 that identified particle production at $y = 0$ in nucleus–nucleus collisions at RHIC can be fully described in their whole $p_{\rm T}$ range and for all centralities by a combination of hydrodynamical (thermal+collective boosted) emission plus (quenched) prompt perturbative production. An exception to this rule are, however, the (anti)protons [58]. Although due to their higher masses, they get an extra push from the hydrodynamic flow up to $p_{\rm T} \sim 3\,{\rm GeV}/c$, for even higher transverse momenta the combination of hydro plus (quenched) pQCD still clearly undershoots the experimental proton spectra. This observation has lent support to the existence of an additional mechanism for baryon production at intermediate $p_{\rm T}$ values ($p_{\rm T} \approx 3$–$5\,{\rm GeV}/c$) based on quark

recombination [59]. This mechanism will not, however, be further considered in this paper since it has no practical implication for photon production and/or for the overall hydrodynamical evolution of the reaction. The overall good theoretical reproduction of the differential $\pi, K, p$ experimental spectra for all centralities is obviously consistent with the previous observation that our calculated total integrated hadron multiplicities agree very well with the experimental data measured at mid-rapidity by the four different RHIC experiments (Fig. 1).

## 3 Direct photon production

As in the case of hadron production, the total direct photon spectrum in a given Au + Au collision at impact parameter $b$ is obtained by adding the primary production from perturbative parton–parton scatterings to the thermal emission rates integrated over the whole space-time volume of the produced fireball. Three sources of direct photons are considered corresponding to each one of the phases of the reaction: prompt production, partonic gas emission, and hadronic gas radiation.

### 3.1 Prompt photons

For the prompt $\gamma$ production we use the NLO pQCD predictions of Vogelsang [60] scaled by the corresponding Glauber nuclear overlap function at $b$, $T_{AA}(b)$, as expected for hard processes in $A+A$ collisions unaffected by final-state effects (as empirically confirmed for photon production in Au + Au [23]). This pQCD photon spectrum is obtained with CTEQ6M [61] parton distribution function (PDF), GRV [62] parametrization of the $q, g \to \gamma$ fragmentation function (FF), and renormalization-factorization scales set equal to the transverse momentum of the photon ($\mu = p_{\rm T}$). Such NLO calculations provide an excellent reproduction of the inclusive direct-$\gamma$ [24] and large-$p_{\rm T}$ $\pi^0$ [25] spectra measured by PHENIX in $p+p$ collisions at $\sqrt{s} = 200\,\text{GeV}$ without any additional parameter (in particular, at variance with results at lower energies [17], no primordial $k_{\rm T}$ is needed to describe the data). We do *not* consider any modification of the prompt photon yields in Au + Au collisions due to partially counteracting initial-state (IS) effects such as: (i) nuclear modifications ("shadowing") of the Au PDF ($< 20\%$, in the relevant $(x, Q^2)$ kinematical range considered here [21, 46, 63]), and (ii) extra nuclear $k_{\rm T}$ broadening (Cronin enhancement) as described e.g. in [20]. Both IS effects are small and/or approximately cancel each other at mid-rapidity at RHIC as evidenced experimentally by the barely modified nuclear modification factor, $R_{d\rm Au} \lesssim 1.1$, for $\gamma$ and $\pi^0$ measured in $d$ + Au collisions at $\sqrt{s_{NN}} = 200\,\text{GeV}$ [64]. Likewise, we do *not* take into account any possible final-state (FS) *photon* suppression due to energy loss of the jet-fragmentation (aka. "anomalous") component of the prompt photon cross section [20, 63, 65, 67], which, if effectively present (see [68] and discussion in Sect. 3.3), can be in principle experimentally determined by detailed measurements of the isolated and non-isolated direct photon baseline spectra in $p+p$ collisions at $\sqrt{s} = 200\,\text{GeV}$ [67].

### 3.2 Thermal photon rates

For the QGP phase we use the most recent full leading order (in $\alpha_{\rm em}$ and $\alpha_{\rm s}$ couplings) emission rates from Arnold et al. [69]. These calculations include hard thermal loop diagrams to all orders and Landau–Migdal–Pomeranchuk (LPM) medium interference effects. The parametrization given in [69] assumes zero net baryon density (i.e. null quark chemical potential, $\mu_{\rm q} = 0$), and *chemical* together with thermal equilibrium. Corrections of the QGP photon rates due to net quark densities are $\mathcal{O}[\mu_{\rm q}^2/(\pi T)^2]$ [70] i.e. marginal at RHIC energies where the baryochemical potential is close to zero at midrapidity ($\mu_{\rm B} = 3\,\mu_{\rm q} \sim 25\,\text{MeV}$) and neglected here. Similarly, although the early partonic phase is certainly not chemically equilibrated (the first instants of the reaction are strongly gluon-dominated) the two main effects from chemical non-equilibrium composition of the QGP: reduction of quark number and increase of the temperature, nearly cancel in the photon spectrum [7, 71] and have not been considered either. For the HRG phase, we use the latest improved parametrization from Turbide et al. [72] which includes hadronic emission processes not accounted for before in the literature. In all calculations, we use a temperature-dependent parametrization of the strong coupling[8], $\alpha_{\rm s}(T) = 2.095/\{\frac{11}{2\pi}\ln(Q/\Lambda_{\overline{\rm MS}}) + \frac{51}{22\pi}\ln[2\ln(Q/\Lambda_{\overline{\rm MS}})]\}$ with $Q = 2\pi T$, obtained from recent lattice results [73].

### 3.3 Extra photon contributions

Apart from the aforementioned (prompt and thermal) photon production mechanisms, Bass et al. [47, 48] have recently evaluated within the Parton Cascade Model (PCM), the contribution to the total Au + Au photon spectrum from secondary (cascading) parton–parton collisions taking place before the attainment of thermalization (i.e. between the transit time of the two nuclei, $\tau \approx 0.15\,\text{fm}/c$, and the standard $\tau_{\rm therm} = 0.6\,\text{fm}/c$ considered at RHIC). Since such cascading light emission is due to second-chance partonic collisions which are, simultaneously, driving the system towards equilibrium, we have decided to account for this contribution within our hydrodynamical evolution alone (such a procedure is not only "acceptable", as discussed in the context of [49, 50], but it is more self-consistent than adding it in an adhoc way from results taken from outside our framework). We achieve this by starting hydrodynamics (whose photon rates also include the expected LPM reduction of the secondary rates [48]) at $\tau_0 = 0.15\,\text{fm}/c$. By doing that, at the same time that we account for this second-chance emission, our initial plasma temperature and associated thermal photon production can be considered to be at their *maximum values* for RHIC energies.

[8] According to this parametrization, $\alpha_S(T) = 0.3$–$0.6$ the range of temperatures of interest here ($T \approx 600$–$150\,\text{MeV}$).

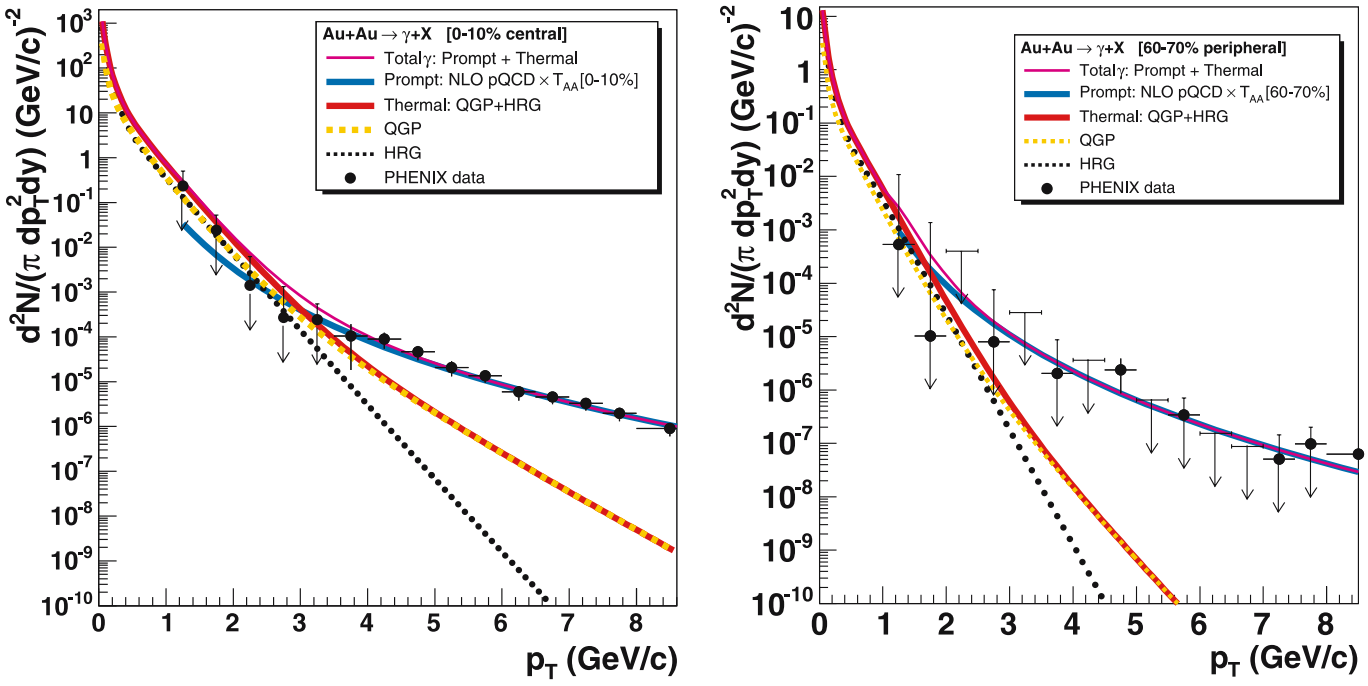


**Fig. 4.** Photon spectra for central (0%–10%, *left*) and peripheral (60%–70%, *right*) Au + Au reactions at $\sqrt{s_{\rm NN}} = 200$ GeV as computed with our hydrodynamical model [with the contributions for the QGP and hadron resonance gas (HRG) given separately] compared to the expected NLO pQCD $p+p$ yields for the prompt $\gamma$ [60] (scaled by the corresponding nuclear overlap function), and to the experimental photon yields measured by the PHENIX collaboration [23]

Likewise, we do not consider the conjectured extra $\gamma$ emission due to the passage of quark jets (Compton-scattering and annihilating) through a dense medium [68, 74, 75], since such a contribution is likely partially compensated by (i) the concurrent non-Abelian energy loss of the parent quarks going through the system [66], plus (ii) a possible *photon* suppression due to energy loss of the "anomalous" component of the prompt photon cross section [20, 63, 65, 67]. As a matter of fact, some approximate cancellation of all those effects must exist since the experimental Au + Au photon spectra above $p_{\rm T} \approx 4$ GeV/$c$ turn out to be well reproduced by primary (pQCD) hard processes alone for all centralities, as can be seen in the comparison of pQCD NLO predictions with PHENIX data [23] (Fig. 4). The apparent agreement between the experimental spectra above $p_{\rm T} \approx 4$ GeV/$c$ and the NLO calculations does not seem to leave much room for extra radiation contributions. A definite conclusion on the existence or not of FS effects on photon production will require in any case precision $\gamma$ data in Au + Au, $d$ + Au and $p+p$ collisions. The more critical issue of the role of the jet bremsstrahlung component needs to be estimated, for example, via measurements of isolated and non-isolated direct photon baseline $p+p$ spectra as discussed in [67]. Additional IS effects not considered so far due, for example, to isospin corrections[9] will require a careful analysis and comparison of Au + Au to reference $d$ + Au photon cross sections too.

### 3.4 Total direct photon spectra

Figure 4 shows our computed total direct photon spectra for central (left) and peripheral (right) Au + Au collisions at $\sqrt{s_{NN}} = 200$ GeV, with the pQCD, QGP, and HRG components differentiated[10]. In central reactions, thermal photon production (mainly of QGP origin) outshines the prompt pQCD emission below $p_{\rm T} \approx 3$ GeV/$c$. Within $p_{\rm T} \approx 1$–$4$ GeV/$c$, thermal photons account for roughly 90% – 50% of the total photon yield in central Au + Au, as can be better seen in the ratio total-$\gamma$/pQCD-$\gamma$ shown in Fig. 5. Photon production in peripheral collisions is, however, clearly dominated by the primary parton–parton radiation. In both cases, hadronic gas emission prevails only for lower $p_{\rm T}$ values. In Fig. 4 we also compare our computed spectra to the inclusive Au + Au photon spectra published recently by the PHENIX collaboration [23]. The total theoretical (pQCD+hydro) differential cross sections are in good agreement with the experimental yields, though for central reactions our calculations tend to "saturate" the upper limits of the data in the range below $p_{\rm T} \approx 4$ GeV/$c$ where thermal photons dominate. New preliminary PHENIX Au + Au direct-$\gamma^*$ results [64, 79] are also systematically above (though still consistent with) these published spectra in the range $p_{\rm T} \approx 1$–$4$ GeV/$c$ and, if confirmed, will bring our results to an even better agreement with the data.

[9] Direct photon cross sections depend on the light quark electric charges and are thus disfavoured in a nucleus target less rich in up quarks than the standard proton reference [77].

[10] We split the mixed phase contribution onto QGP and HRG components calculating the relative proportion of QGP (HRG) matter in it.

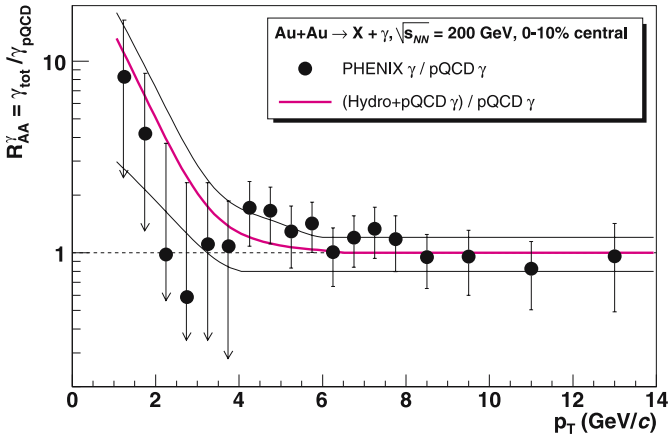


**Fig. 5.** Direct photon "nuclear modification factor", $R^{\gamma}_{AA}$, see (2), obtained as the ratio of the total over the prompt $\gamma$ spectra for 0%–10% most central Au + Au reactions at $\sqrt{s_{\rm NN}} = 200$ GeV. The *solid line* is the ratio resulting from our hydro+pQCD model. The points show the PHENIX data [23] over the same NLO yields and the *dashed-dotted curves* indicate the theoretical uncertainty of the NLO calculations (see text)

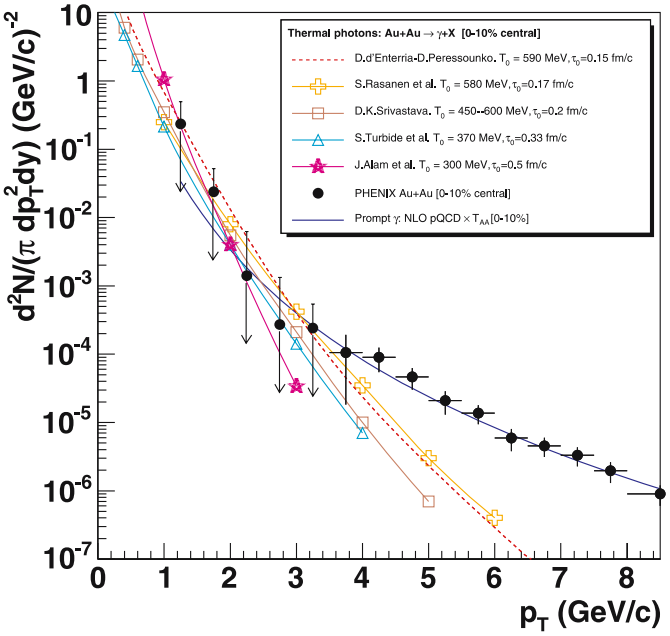


**Fig. 6.** Thermal photon predictions for central Au + Au reactions at $\sqrt{s_{\rm NN}} = 200$ GeV as computed with different hydrodynamical [10, 11, 14] or "dynamical fireball" [72] models, compared to (i) our hydro calculations (*dashed curve*), (ii) the expected perturbative $\gamma$ yields ($T_{AA}$-scaled NLO $p+p$ calculations [60]), and (iii) the experimental total direct photon spectrum measured by PHENIX [23]

To better distinguish the relative amount of thermal radiation in the theoretical and experimental *total* direct photon spectra in central Au + Au collisions, we present in Fig. 5 the nuclear modification factor $R^{\gamma}_{AA}$ defined as the ratio of the total over prompt (i.e. $T_{AA}$-scaled $p+p$ pQCD predictions) photon yields:

$$R^{\gamma}_{AA}(p_{\rm T}) = \frac{{\rm d}N^{\rm total\,\gamma}_{\rm AuAu}/{\rm d}p_{\rm T}}{T_{AA}{\rm d}\sigma^{\gamma\,\rm pQCD}_{\rm pp}/{\rm d}p_{\rm T}}. \qquad (2)$$

A value $R^{\gamma}_{AA} \approx 1$ would indicate that all the photon yield can be accounted for by the prompt production alone. Of course, since our total direct-$\gamma$ result for central Au + Au includes thermal emission from the QGP and HRG phases, we theoretically obtain $R^{\gamma}_{AA} \approx 10$–$1$ in the $p_{\rm T} \approx 1$–$4$ GeV/$c$ region where the thermal component is significant (Fig. 5). In this very same $p_{\rm T}$ range, although the available PHENIX results have still large uncertainties[11], the central value of most of the data points is clearly consistent with the existence of a significant excess over the NLO pQCD expectations. A note of caution is worth here, however, regarding the $R^{\gamma}_{AA} \gg 1$ value observed for both the theoretical and experimental spectra below $p_{\rm T} \approx 4$ GeV/$c$, since it is not yet clear to what extent the NLO predictions, entering in the denominator of (2), are realistic in this thermal-photon "region of interest". Indeed, in this comparatively low $p_{\rm T}$ range the theoretical prompt yields are dominated by the jet bremsstrahlung contribution [67] which is intrinsically non-perturbative (i.e. not computable) and determined solely from the parametrized parton-to-photon GRV [62] FF which is relatively poorly known in this kinematic range.

The standard scale uncertainties in the NLO pQCD calculations are $\pm 20\%$ above $p_{\rm T} \approx 4$ GeV/$c$ but we have assigned a much more pessimistic $^{-200}_{+50}\%$ uncertainty to these calculations in the range $p_{\rm T} \approx 1$–$4$ GeV/$c$ (dashed-dotted lines in Fig. 5). Precise measurements of the direct-$\gamma$ baseline spectrum in $p+p$ collisions at $\sqrt{s} = 200$ GeV above $p_{\rm T} = 1$ GeV/$c$ are mandatory before any definite conclusion can be drawn on the existence or not of a thermal excess from the Au + Au experimental data.

As a final cross-check of our computed hydrodynamical photon yields, we have compared them to previously published predictions for thermal photon production in Au + Au collisions at top RHIC energy: Srivastava et al. [10] (with initial conditions $\tau_0 \approx 0.2$ fm/$c$ and $T_0 \approx 450$–$660$ MeV), Jan-e Alam et al.[12] [11] ($\tau_0 = 0.5$ fm/$c$ and $T_0 = 300$ MeV), Steffen and Thoma [13] ($\tau_0 = 0.5$ fm/$c$ and $T_0 = 300$ MeV), Rasanen et al. [14] ($\tau_0 = 0.17$ fm/$c$ and $T_0 = 580$ MeV), Hammon et al. [46] ($\tau_0 = 0.12$ fm/$c$ and $T_0 = 533$ MeV), and Turbide et al.[13] [72] ($\tau_0 = 0.33$ fm/$c$ and $T_0 = 370$ MeV). For similar initial conditions, the computed total thermal yields in those works are compatible within a factor of $\sim 2$ with those presented here. Some

[11] Technically, the PHENIX data points below $p_{\rm T} = 4$ GeV/$c$ have "lower errors that extend to zero", i.e. a non-zero direct-$\gamma$ signal is indeed observed in the data but the associated errors are larger than the signal itself [23].

[12] Alam et al. have recently [78] recomputed their hydrodynamical yields using higher initial temperatures ($T_0 = 400$ MeV at $\tau_0 = 0.2$ fm/$c$) and getting a better agreement with the data.

[13] Note that *stricto senso* Turbide's spectra are not obtained with a pure hydrodynamical computation but using a simpler "dynamical fireball" model which assumes constant acceleration in longitudinal and transverse directions.

of those predictions are shown in Fig. 6 confronted to our calculations. Our yields are, in general, above all other predictions since, as aforementioned, both our initial thermalization time and energy densities (temperatures) have the most "extreme" values possible consistent with the RHIC charged hadron multiplicities. They agree specially well with the hydrodynamical calculations of the Jyväskylä group [14] which have been computed with the same up-to-date QGP rates used here. Given the current (large) uncertainties of the available published data, all thermal photon predictions are consistent with the experimental results. However, as aforementioned, newer (preliminary) PHENIX direct-$\gamma^{\star}$ measurements have been reported very recently [64, 79] and indicate a clear excess of direct photons over NLO pQCD for Au + Au at $\sqrt{s_{NN}} = 200\,\mathrm{GeV}$ in this $p_{\mathrm{T}}$ range in excellent agreement with our thermal photon calculations.

## 4 Thermal photons and the QCD equation-of-state

In order to experimentally isolate the thermal photon spectrum one needs to subtract from the total direct-$\gamma$ spectrum the non-equilibrated "background" of prompt photons. The prompt $\gamma$ contribution emitted in a given Au + Au centrality can be measured separately in reference $p+p$ (or $d+\mathrm{Au}$) collisions at the same $\sqrt{s}$, scaled by the corresponding nuclear overlap function $T_{AA}(b)$, and subtracted from the total Au + Au $\gamma$ spectrum [67]. The simpler expectation is that the remaining photon spectrum for a given impact parameter $b$

$$\frac{\mathrm{d}N^{\mathrm{thermal}\gamma}_{\mathrm{AuAu}}(b)}{\mathrm{d}p_{\mathrm{T}}} = \frac{\mathrm{d}N^{\mathrm{total}\gamma}_{\mathrm{AuAu}}(b)}{\mathrm{d}p_{\mathrm{T}}} - T_{AA}(b)\frac{\mathrm{d}\sigma^{\gamma}_{\mathrm{pp}}}{\mathrm{d}p_{\mathrm{T}}}\,, \qquad (3)$$

will be just that due to thermal emission from the partonic and hadronic phases of the reaction. Such a subtraction procedure can be effectively applied to all the $\gamma$ spectra measured in different centralities as long as both the total Au + Au and baseline $p+p$ photon spectra are experimentally measured with reasonable ($\lesssim 15\%$) point-to-point (systematical and statistical) uncertainties [67]. The subtracted spectra (3) can be therefore subject to scrutiny in terms of the thermodynamical properties of the radiating medium.

### 4.1 Determination of the initial temperature

Due to their weak electromagnetic interaction with the surrounding medium, photons produced in the reaction escape freely the interaction region immediately after their production. Thus, even when emitted from an equilibrated source, they are not reabsorbed by the medium and do not have a black-body spectrum at the source temperature. Nonetheless, since all the theoretical thermal $\gamma$ rates [69, 72] have a general functional dependence of the form[14] $E_{\gamma}\,\mathrm{d}R_{\gamma}/\mathrm{d}^3p \propto T^2\exp\left(-E_{\gamma}/T\right)$, one would expect the final spectrum to be locally exponential with an inverse slope parameter strongly correlated with the (local) temperature $T$ of the radiating medium.

Obviously, such a general assumption is complicated by several facts. On the one hand, the final thermal photon spectrum is a sum of exponentials with different temperatures resulting from emissions at different time-scales and/or from different regions of the fireball which has strong temperature gradients (the core being much hotter than the "periphery"). On the other hand, collective flow effects (stronger for increasingly central collisions) superimpose on top of the purely thermal emission leading to an effectively larger inverse slope parameter ($T_{\mathrm{eff}} \approx \sqrt{(1+\beta)/(1-\beta)}\,T$) [12]. One of the main results of this paper is to show that, based upon a realistic hydrodynamical model, such effects do not destroy completely the correlation between the apparent photon temperature and the maximal temperature actually reached at the beginning of the collision process. We will show that such a correlation indeed exists and that the local inverse slope parameter obtained by fitting to an exponential, at high enough $p_{\mathrm{T}}$, the thermal photon spectrum obtained via the expression (3), indeed provides a good proxy of the initial temperature of the system without much distortion due to collective flow (and other) effects.

To determine to what extent the thermal slopes are indicative of the original temperature of the system, we have fitted the thermal spectra obtained from our hydrodynamical calculations in different Au + Au centralities to an exponential distribution in different $p_{\mathrm{T}}$ ranges. Since, – according to our Glauber prescription for the impact-parameter dependence of the hydrodynamical initial conditions –, different centralities result in different initial energy densities, we can in this way explore the dependence of the apparent thermal photon temperature on the maximal initial temperatures $T_0$ (at the core) of the system. The upper plot of Fig. 7 shows the obtained local slope parameter, $T_{\mathrm{eff}}$, as a function of the initial temperature $T_0$ for our default QGP+HRG hydrodynamical evolution (Table 1). We find that although all the aforementioned effects smear the correlation between the apparent and original temperatures, they do not destroy it completely. The photon slopes are indeed approximately proportional to the initial temperature of the medium, $T_0$. There is also an obvious anti-correlation between the $p_{\mathrm{T}}$ of the radiated photons and their time of emission. At high enough $p_{\mathrm{T}}$ the hardest photons issuing from the hottest zone of the system swamp completely any other softer contributions emitted either at later stages and/or from outside the core region of the fireball.

Thus, the higher the $p_{\mathrm{T}}$ range, the closer is $T_{\mathrm{eff}}$ to the original $T_0$ at the center of the system. According to our calculations, empirical thermal slopes measured above $p_{\mathrm{T}} \approx 4\,\mathrm{GeV}/c$ in central Au + Au collisions are above $\sim 400\,\mathrm{MeV}$ i.e. only $\sim 30\%$ lower than the "true" maximal (local) temperature of the quark-gluon phase. On the

[14] The $T^2$ factor is just an overall normalization factor in this case (since its temporal variation is small compared to the short emission times) and does not significantly alter the exponential shape of the spectra.

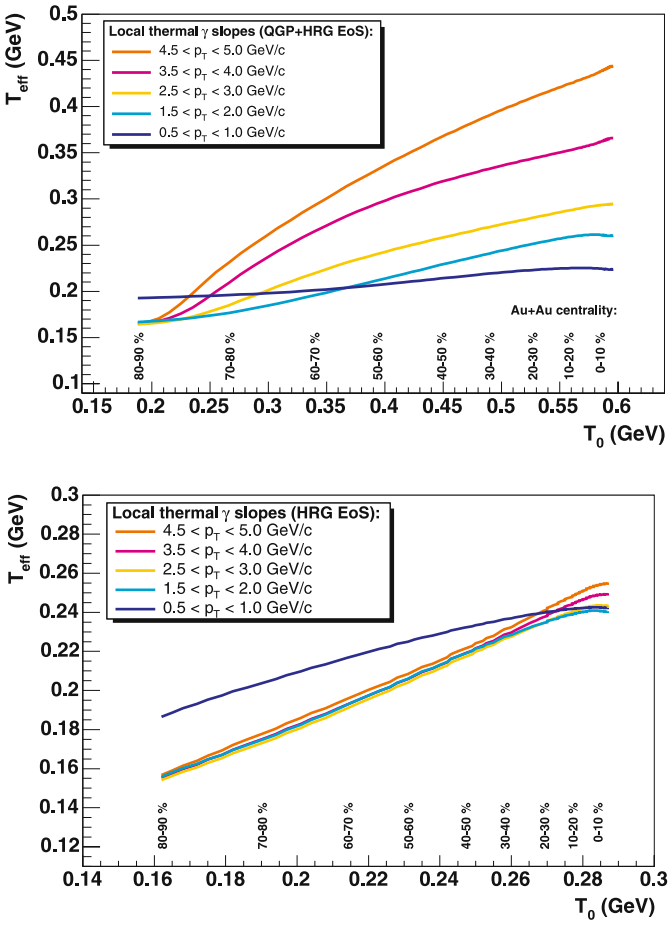


**Fig. 7.** Local photon slope parameters $T_{\rm eff}$ (obtained from exponential fits of the thermal photon spectrum in different $p_{\rm T}$ ranges) plotted versus the initial (maximum) temperature $T_0$ of the fireball produced at different centralities in Au + Au collisions at $\sqrt{s} = 200$ GeV. *Upper plot* hydrodynamical calculations with QGP+HRG EoS (Table 1), *bottom* HRG EoS (with initial conditions $\varepsilon_0 = 30\,{\rm GeV/fm^3}$ at $\tau_0 = 0.6\,{\rm fm/c}$)

other hand, local $\gamma$ slopes in the range below $p_{\rm T} \approx 1\,{\rm GeV}/c$ have almost constant value $T_{\rm eff} \sim 200\,{\rm MeV}$ (numerically close to $T_{\rm crit}$) for all centralities and are almost insensitive to the initial temperature of the hydrodynamical system but mainly specified by the exponential prefactors in the hadronic emission rates, plus collective boost effects.

To assess the dependence of the thermal photon spectra on the underlying EoS, we have rerun our hydro evolution with just the EoS of a hadron resonance gas. We choose now as initial conditions $\varepsilon_0 = 30\,{\rm GeV/fm^3}$ at $\tau_0 = 0.6\,{\rm fm}/c$, which can still reasonably describe the experimental hadron spectra. Obviously, any description in terms of hadronic degrees of freedom at such high energy densities is unrealistic but we are interested in assessing the effect on the thermal photon slopes of a non ideal-gas EoS as e.g. that of a HRG-like system with a large number of heavy resonances (or more generally, of any EoS with exponentially rising number of mass states).

The photon slopes for the pure HRG gas EoS (Fig. 7, bottom) are lower ($T_{\rm eff}^{\rm max} \approx 220\,{\rm MeV}$) than in the default QGP+HRG evolution, not only because the input HRG $\varepsilon_0$ is smaller (the evolution starts at a later $\tau_0$) but, specially because for the same initial $\varepsilon_0$ the effective number of degrees of freedom in a system with a HRG EoS is higher than that in a QGP[15] and therefore the initial temperatures are lower. A second difference is that, for all $p_{\rm T}$ ranges, we find almost the same exact correlation between the local $\gamma$ slope and $T_0$, indicating a single underlying (hadronic) radiation mechanism dominating the transverse spectra at all $p_{\rm T}$.

Two overall conclusions can be obtained from the study of the hydrodynamical photon slopes. First, the observation in the data, via (3), of a thermal photon excess above $p_{\rm T} \approx 2.5\,{\rm GeV}/c$ with exponential slope $T_{\rm eff} \gtrsim 250\,{\rm MeV}$ is an unequivocal proof of the formation of a system with maximum temperatures above $T_{\rm crit}$ since no realistic collective flow mechanism can generate such a strong boost of the photon slopes, while simultaneously reproducing the hadron spectra. Secondly, pronounced $p_{\rm T}$ dependences of the local thermal slopes seem to be characteristic of space-time evolutions of the reaction that include an ideal-gas QGP radiating phase.

### 4.2 Determination of the QCD Equation of State (EoS)

As we demonstrated in the previous section, $T_{\rm eff}$ is approximately proportional to the maximum temperature reached in a nucleus–nucleus reaction. One can go one step further beyond the mere analysis of the thermal photon slopes and try to get a direct handle on the equation of state of the radiating medium by looking at the correlation of $T_{\rm eff}$ with experimental observables related to the initial energy or entropy densities of the system. For example, assuming an isentropic expansion (which is implicit in our perfect fluid hydrodynamical equations with zero viscosity) one can estimate the *initial* entropy density $s$ at the time of photon emission from the total *final* particle multiplicity ${\rm d}N/{\rm d}y$ measured in the reaction. Varying the centrality of the collision, one can then explore the form of the dependence $s = s(T)$ at the first instants of the reaction, extract the underlying equation of state of the radiating system and trace any signal of a possible phase transition. Indeed, the two clearest pieces of evidence of QGP formation from QCD calculations on the lattice are (i) the sharp rise of $\varepsilon(T)/T^4$, or equivalently of $s(T)/T^3$, at temperatures around $T_{\rm crit}$, and (ii) the flattening of the same curve above $T_{\rm crit}$. The sharp jump is of course due to the sudden release of a large number of (partonic) degrees of freedom at $T_{\rm crit}$. The subsequent plateau is due to the full formation of a QGP with a *fixed* (constant) number of degrees of freedom.

We propose here to use $T_{\rm eff}$ as a proxy for the initial temperature of the system, and directly study the evolution, versus $T_{\rm eff}$, of the effective number of degrees of free-

[15] Note that $g(T) \propto \varepsilon/T^4$ increases exponentially with $T$ for a HRG-like EoS, and at high enough temperatures will clearly overshoot the QGP constant number of degrees of freedom.

dom defined as[16]

$$g(s,T) = \frac{\pi^2}{4\,\zeta(4)}\frac{s}{T^3}\,(\hbar c)^3 = \frac{45}{2\pi^2}\,\frac{s}{T^3}(\hbar c)^3, \qquad (4)$$

which coincides with the degeneracy of a weakly interacting gas of massless particles. [In a similar avenue, Muller and Rajagopal [80] have recently proposed a method to estimate the number of thermodynamic degrees of freedom via $g_{\rm eff} \propto s^4/\epsilon^3$, where $s$ is also determined from the final hadron multiplicities.] The dashed line in Fig. 8 (top) shows the evolution of the *true* number of degrees of freedom $g_{\rm hydro}(s_0, T_0)$ computed via (4), as a function of the (maximal) temperatures and entropies directly obtained from the initial conditions of our hydrodynamical model in different Au + Au centralities[17]. The first thing worth to note is that $g(s,T)$ remains constant at the expected degeneracy $g_{\rm hydro} = 42.25$ of an ideal gas of $N_{\rm f} = 2.5$ quarks and gluons for basically *all* the maximum temperatures accessible in the different centralities of Au + Au at $\sqrt{s_{NN}} = 200$ GeV. This indicates that at top RHIC energies and for most of the impact parameters, $T_0$ is (well) above $T_{\rm crit}$ and the hottest parts of the initial fireball are in the QGP phase. The expected drop in $g_{\rm hydro}$ related to the transition to the hadronic phase is only seen, if at all, for the very most peripheral reactions (with $T_0 \approx T_c$). Thus, direct evidence of the QGP-HRG phase change itself via the study of the centrality dependence of any experimentally accessible observable would only be potentially feasible at RHIC in Au + Au reactions at *lower* center-of-mass energies [81].

As aforementioned, we can empirically trace the QCD EoS shown in Fig. 8 (and eventually determine the temperature-evolution of the thermodynamic degrees of freedom of the produced medium) using the estimate of the initial temperature given by the thermal photon slopes, $T_{\rm eff}$, and a second observable closely related to the initial entropy of the system such as the final-state hadron multiplicity, $\mathrm{d}N/\mathrm{d}y$. Although one could have also considered to obtain $g_{\rm eff}$ via $\varepsilon/T^4 \propto (\mathrm{d}E_{\rm T}/\mathrm{d}y)/T^4_{\rm eff}$, using the transverse energy per unit rapidity $\mathrm{d}E_{\rm T}/\mathrm{d}y$ measured in different Au + Au centralities [41], we prefer to use the expression (4) which contains the entropy – rather than the energy – density for two reasons:

(i) the experimentally accessible values of $\mathrm{d}N/\mathrm{d}y$ remain constant in an isentropic expansion (i.e. $\mathrm{d}N/\mathrm{d}y \propto s_0$) whereas, due to longitudinal work, the measured final $\mathrm{d}E_{\rm T}/\mathrm{d}y$ provides only a *lower limit* on the initial $\varepsilon$; and

(ii) $g_{\rm eff} \propto s/T^3_{\rm eff}$ is less sensitive to experimental uncertainties associated to the measurement of $T_{\rm eff}$ than $g_{\rm eff} \propto \varepsilon/T^4_{\rm eff}$ is.

Again, in the absence of dissipative effects, the space-time evolution of the produced system in a nucleus–nucleus reaction is isentropic and the entropy density (per unit rapidity) at the thermalization time $\tau_0$ can be directly connected (via $s \approx 4\varrho$ [82]) to the final charged hadron pseudo-rapidity density[18]:

$$s \approx 4\frac{\mathrm{d}N}{\mathrm{d}V} \approx \frac{7.2}{\langle A_\perp\rangle\,\tau_0}\frac{\mathrm{d}N_{\rm ch}}{\mathrm{d}\eta}, \qquad (5)$$

where we have written the volume of the system, $\mathrm{d}V = \langle A_\perp\rangle\,\tau_0\,\mathrm{d}\eta$, as the product of the (purely geometrical) average transverse overlap area for each centrality times the starting proper time of our hydro evolution ($\tau_0 = 0.15\,\mathrm{fm}/c$), and where $\mathrm{d}N_{\rm ch}/\mathrm{d}\eta$ is the *charged* hadron

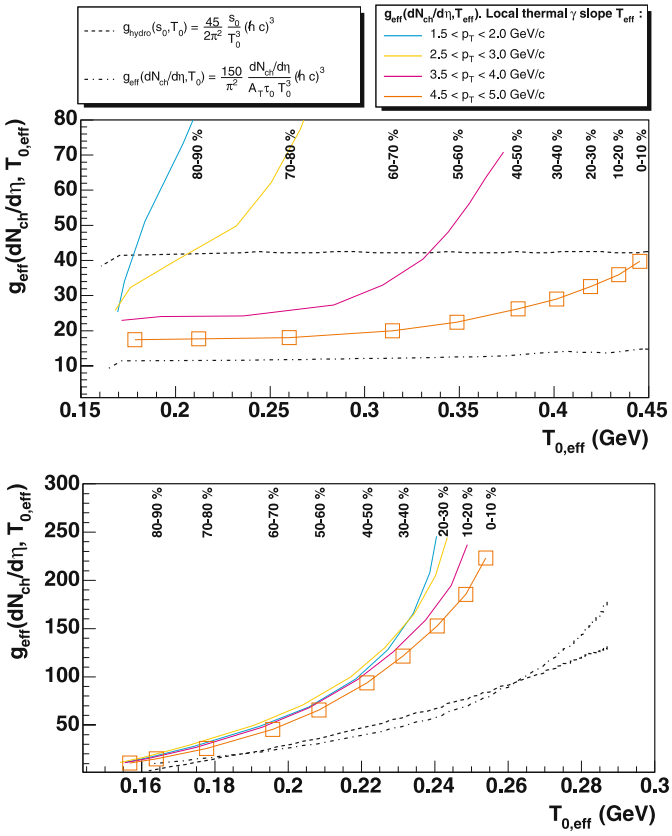


**Fig. 8.** Effective initial number of degrees of freedom obtained from our hydrodynamical calculations with a QGP+HRG EoS (*upper plot*), and with a pure HRG EoS (*bottom*), plotted as a function of the temperature ($T_0$) or thermal photon slope ($T_{\rm eff}$) in different Au + Au centrality classes at $\sqrt{s_{\rm NN}} = 200$ GeV. The number of degrees of freedom are computed respectively: (i) from our initial thermodynamical conditions ($s_0$, $T_0$) via (4) (*dashed line*), (ii) from the obtained charged hadron multiplicity $\mathrm{d}N_{\rm ch}/\mathrm{d}\eta$ and the *true* initial temperature $T_0$ via (6) (*dotted-dashed line*); and (iii) from $\mathrm{d}N_{\rm ch}/\mathrm{d}\eta$ and the thermal photon slopes $T_{\rm eff}$ measured in different $p_{\rm T}$ ranges via (6) (*solid lines*). For illustrative purposes, the *open squares* indicate the approximate position of the different Au + Au centrality classes (in 10% percentiles) for the values of $g_{\rm eff}$ obtained using the thermal photon slopes measured above $p_{\rm T} = 4\,\mathrm{GeV}/c$

[16] Units are in GeV and fm. $\zeta(4) = \pi^4/90$, where $\zeta(n)$ is the Riemann zeta function.

[17] In the most peripheral reactions, the bag entropy has been subtracted to make more apparent the drop near $T_c$.

[18] This formula uses $N_{\rm tot}/N_{\rm ch} = 3/2$, and the Jacobian $|\mathrm{d}\eta/\mathrm{d}y| = E/p \approx 1.2$.

multiplicity customarily measured experimentally at mid-rapidity[19]. By combining (4) and (5), we obtain an estimate for the number of degrees of freedom of the system produced in a given $A+A$ collision at impact parameter $b$:

$$g_{\rm eff}\left(\frac{{\rm d}N_{\rm ch}(b)}{{\rm d}\eta},\, T_{\rm eff}(b)\right) \approx \frac{150}{\pi^2}\frac{(\hbar c)^3}{\langle A_\perp(b)\rangle\,\tau_0 T_{\rm eff}^3(b)}\frac{{\rm d}N_{\rm ch}(b)}{{\rm d}\eta}\,, \tag{6}$$

which can be entirely determined with two experimental observables: ${\rm d}N_{\rm ch}/{\rm d}\eta$ and $T_{\rm eff}$.

Let us first assess to what extent the ansatz (6) is affected by the assumption that (5) indeed provides a good experimental measure of the initial entropy density $s$. The dotted-dashed curve in Fig. 8 has been obtained via (6) using the $({\rm d}N_{\rm ch}/{\rm d}\eta)/\langle A_\perp\rangle$ values obtained from our hydrodynamical model, and the *true* (input) initial temperature of the system $T_0$, and thus it is only sensitive to the way we estimate the entropy density. The resulting curve is a factor of $\sim 3$ below the expected "true" $g_{\rm hydro}$ curve, i.e. $g_{\rm eff}\,({\rm d}N_{\rm ch}/{\rm d}\eta, T_0) \approx 3 g_{\rm hydro}(s_0, T_0)$, indicating that (6) underestimates by the same amount the maximal entropy of the original medium. This is so because our estimate $({\rm d}N_{\rm ch}/{\rm d}\eta)/\langle A_\perp\rangle$ specifies the entropy density averaged over the *whole* transverse area $\langle A_\perp\rangle$, whereas the maximal entropy area in the *core* of the system (from where the hardest thermal photons are emitted) is $\sim 3$ times *smaller*. Although one could think of a method to correct for this difference, this would introduce an extra model-dependence that we want to avoid at this point. We prefer to maintain the simple (geometrical overlap) expression of the transverse area $\langle A_\perp(b)\rangle$ in (6), and exploit the fact that, although such an equation does not provide the true *absolute* number of degrees of freedom, it does provide a very reliable indication of the dependence of $g_{\rm eff}$ on the temperature of the system and, therefore, of the exact *form* of the underlying EoS.

Finally, let us consider the last case where we use (6) with the values of ${\rm d}N_{\rm ch}/{\rm d}\eta$ *and* $T_{\rm eff}$ that can be actually experimentally measured. The different solid curves in the upper plot of Fig. 8 show the effective degeneracy $g_{\rm eff}$, computed using (6) and the local photon slopes $T_{\rm eff}$ measured in different $p_{\rm T}$ ranges for our default QGP+HRG evolution. As one could expect from Fig. 7, the best reproduction of the shape of the underlying EoS is obtained with the effective temperatures measured in higher $p_{\rm T}$ bins. For those $T_{\rm eff}$, the computed $g_{\rm eff}$'s show a relatively constant value in a wide range of centralities as expected for a weakly interacting QGP. Deviations from this ideal-gas plateau appear for more central collisions, due to an increasing difference between the (high) initial temperatures, $T_0$, and the apparent temperature given by the photon slopes (Fig. 7). Such deviations do not spoil, however, the usefulness of our estimate since, a non-QGP EoS would result in a considerably different dependence of $g_{\rm eff}$ on the reaction centrality. Indeed, the different curves in the bottom plot of Fig. 8 obtained with a pure hadron resonance gas EoS clearly indicate[20] that a HRG EoS, or in general any EoS with exponentially increasing number of mass states, would bring about a much more dramatic rise of $g_{\rm eff}$ with $T_{\rm eff}$.

In summary, the estimate (6) indeed provides a direct experimental handle on the *form* of the EoS of the strongly interacting medium produced in the first instants of high-energy nuclear collisions. More quantitative conclusions on the possibility to extract the exact shape of the underlying EoS and/or the absolute number of degrees of freedom of the produced medium require more detailed theoretical studies (e.g. with varying lattice-inspired EoS's [81] and/or using more numerically involved 3D+1 hydrodynamical approaches). In any case, we are confident that by experimentally measuring the thermal photon slopes in different Au + Au centralities and correlating them with the associated charged hadron multiplicities as in (6), one can approximately observe the expected "plateau" in the number of degrees of freedom indicative of QGP formation above a critical value of $T$.

## 5 Conclusions

We have studied thermal photon production in Au + Au reactions at $\sqrt{s_{NN}} = 200$ GeV using a Bjorken hydrodynamic model with longitudinal boost invariance. We choose the initial conditions of the hydrodynamical evolution so as to efficiently reproduce the observed particle multiplicity in central Au + Au collisions at RHIC and use a simple Glauber prescription to obtain the corresponding initial conditions for all other centralities. With such a model we can perfectly reproduce the identified soft pion, kaon and proton $p_{\rm T}$-differential spectra measured at RHIC. Complementing our model with the most up-to-date parametrizations of the QGP and HRG thermal photon emission rates plus a NLO pQCD calculation of the prompt $\gamma$ contribution, we obtain direct photon spectra which are in very good agreement with the Au + Au direct photon (upper limit) yields measured by the PHENIX experiment. In central collisions, a thermal photon signal should be identifiable as a factor of $\sim 8$–$1$ excess over the pQCD $\gamma$ component within $p_{\rm T} \approx 1$–$4$ GeV/$c$, whereas pure prompt emission clearly dominates the photon spectra at all $p_{\rm T}$ in peripheral reactions. The local inverse slope parameter of the thermal photon spectrum is found to be directly correlated to the maximum temperature attained in the course of the collision. The experimental measurement of local thermal photon slopes above $p_{\rm T} \approx 2.5$ GeV/$c$, with values $T_{\rm eff} \gtrsim 250$ MeV and with pronounced $p_{\rm T}$ dependences can only be reproduced by space-time evolutions of the reaction that include a QGP phase.

Finally, we have proposed and tested within our framework an empirical method to determine the effective ther-

[19] Note again that both the photon slopes and the charged hadron multiplicities are proxies of the thermodynamical conditions of the system *at the same time* $\tau_0$.

[20] Accidentally, $g_{\rm eff} \gtrsim g_{\rm hydro}$ in the case of a HRG EoS, because the underestimation of the apparent temperature (raised to the cube) compensates for the aforementioned area averaging of the entropy.

modynamical number of degrees of freedom of the produced medium, $g(s,T) \propto s(T)/T^3$, by correlating the thermal photon slopes with the final-state charged hadron multiplicity measured in different centrality classes. We found that one can clearly distinguish between the equation of state of a weakly interacting quark-gluon plasma and that of a system with rapidly rising number of mass states with $T$. Stronger quantitative conclusions on the exact shape of the underlying EoS and/or the absolute number of degrees of freedom of the produced medium require more detailed theoretical studies as well as high precision photon data in Au + Au and baseline $p+p$, $d+$ Au collisions. In any case, the requirement for hydrodynamical models of concurrently describing the experimental bulk hadron and thermal photon spectra for different Au + Au centralities at $\sqrt{s_{NN}} = 200\,\mathrm{GeV}$, imposes very strict constraints on the form of the equation of state of the underlying expanding QCD matter produced in these reactions.

*Acknowledgements.* We would like to thank Werner Vogelsang for providing us with his NLO pQCD calculations for photon production in $p+p$ collisions at $\sqrt{s} = 200\,\mathrm{GeV}$; Sami Rasanen for valuable comments on hydrodynamical photon production; and Helen Caines and Olga Barannikova for useful discussions on (preliminary) STAR hadron data. D.P. acknowledges support from MPN of Russian Federation under grant NS-1885.2003.2.

## References

1. See e.g. F. Karsch, Lect. Notes Phys. **583**, 209 (2002)
2. U.W. Heinz, M. Jacob, nucl-th/0002042
3. M. Gyulassy, L. McLerran, Nucl. Phys. A **750**, 30 (2005)
4. E.L. Feinberg, Nuovo Cim. A **34**, 391 (1976)
5. E.V. Shuryak, Phys. Lett. B **78**, 150 (1978) [Sov. J. Nucl. Phys. **28**, 408 (1978); YAFIA, **28**, 796 (1978)]
6. T. Peitzmann, M.H. Thoma, Phys. Rept. **364**, 175 (2002)
7. F. Arleo et al., in "CERN Yellow Report on Hard Probes in Heavy Ion Collisions at the LHC"; hep-ph/0311131
8. C. Gale, K.L. Haglin, in Quark Gluon Plasma, Vol 3, ed. by R.C. Hwa, X.N. Wang (World Scientific, Singapore), [hep-ph/0306098]
9. WA98 Collaboration, M.M. Aggarwal et al., Phys. Rev. Lett. **85**, 3595 (2000)
10. D.K. Srivastava, B. Sinha, Phys. Rev. C **64**, 034902 (2001); D.K. Srivastava, Pramana **57**, 235 (2001)
11. J.-e. Alam, S. Sarkar, T. Hatsuda, T.K. Nayak, B. Sinha, Phys. Rev. C **63**, 021901 (2001)
12. D.Y. Peressounko, Y.E. Pokrovsky, Nucl. Phys. A **624**, 738 (1997); Nucl. Phys. A **669**, 196 (2000); hep-ph/0009025
13. F.D. Steffen, M.H. Thoma, Phys. Lett. B **510**, 98 (2001)
14. P. Huovinen, P.V. Ruuskanen, S.S. Rasanen, Phys. Lett. B **535**, 109 (2002); S.S. Rasanen, Nucl. Phys. A **715**, 717 (2003); H. Niemi, S.S. Rasanen, P.V. Ruuskanen in [7]
15. D. d'Enterria, Phys. Lett. B **596**, 32 (2004)
16. P. Aurenche, M. Fontannaz, J.P. Guillet, B.A. Kniehl, E. Pilon, M. Werlen, Eur. Phys. J. C **9** 107 (1999)
17. C.Y. Wong, H. Wang, Phys. Rev. C **58**, 376 (1998)
18. L. Apanasevich et al., Phys. Rev. D **63**, 014009 (2001)
19. J.W. Cronin et al., Phys. Rev. D **11**, 3105 (1975); D. Antreasyan et al., Phys. Rev. D **19**, 764 (1979)
20. A. Dumitru, N. Hammon, hep-ph/9807260; A. Dumitru, L. Frankfurt, L. Gerland, H. Stocker, M. Strikman, Phys. Rev. C **64**, 054909 (2001)
21. S. Jeon, J. Jalilian-Marian, I. Sarcevic, Nucl. Phys. A **715**, 795 (2003)
22. G. Papp, G.I. Fai, P. Levai, hep-ph/9904503
23. PHENIX Collaboration, J. Frantz, J. Phys G **30**, S1003 (2004); PHENIX Collaboration, S.S. Adler et al., Phys. Rev. Lett. **94**, 232301 (2005)
24. PHENIX Collaboration, K. Okada, Proceed. SPIN'04 [hep-ex/0501066]; PHENIX Collaboration, S.S. Adler et al., Phys. Rev. D **71**, 071102 (2005)
25. PHENIX Collaboration, S.S. Adler et al., Phys. Rev. Lett. **91**, 241803 (2003)
26. PHENIX Collaboration, S.S. Adler et al., Phys. Rev. Lett. **91**, 072303 (2003); PHENIX Collaboration, H. Buesching, nucl-ex/0410002
27. P.F. Kolb, U. Heinz, in Quark Gluon Plasma, Vol 3, ed. by R.C. Hwa, X.N. Wang, (World Scientific, Singapore); [nucl-th/0305084], and refs. therein.
28. D. Teaney, J. Lauret, E.V. Shuryak, nucl-th/0110037
29. T. Hirano, K. Tsuda, Phys. Rev. C **66**, 054905 (2002); T. Hirano, Y. Nara, Phys. Rev. C **69**, 034908 (2004)
30. J.D. Bjorken, Phys. Rev. D **27**, 140 (1983)
31. BRAHMS Collaboration, I.G. Bearden et al., Phys. Rev. Lett. **94**, 162301 (2005); BRAHMS Collaboration, I. Arsene et al.,Phys. Rev. C **72**, 014908 (2005)
32. K.J. Eskola, K. Kajantie, P.V. Ruuskanen, Eur. Phys. J. C **1**, 627 (1998)
33. B. Mohanty and J.-e. Alam, Phys. Rev. C **68**, 064903 (2003)
34. R.W. MacCormack, A.J. Paullay, Computers and Fluids, Vol. 2 (Pergamon, Oxford 1974)
35. P. Braun-Munzinger, K. Redlich, J. Stachel, in Quark Gluon Plasma., Vol 3, ed. by R.C. Hwa, X.N. Wang, (World Scientific, Singapore), [nucl-th/0304013]
36. A. Andronic, P. Braun-Munzinger, J. Stachel, nucl-th/0511071
37. F. Cooper, G. Frye, Phys. Rev. D **10**, 186 (1974)
38. Particle Data Group Collaboration, K. Hagiwara et al., Phys. Rev. D **66**, 010 001 (2002)
39. B. Hahn, D.G. Ravenhall, R. Hofstadter, Phys. Rev. **101**, 1131 (1956)
40. P.F. Kolb, U.W. Heinz, P. Huovinen, K.J. Eskola, K. Tuominen, Nucl. Phys. A **696**, 197 (2001)
41. PHENIX Collaboration, S.S. Adler et al., Phys. Rev. C **71**, 034 908 (2005) [Erratum-ibid. C **71**, 049 901 (2005)]
42. STAR Collaboration, T.S. Ullrich, Heavy Ion Phys. **21**, 143 (2004)
43. PHOBOS collaboration, B.B. Back et al., Nucl. Phys. A **715**, 65 (2003)
44. BRAHMS Collaboration, I.G. Bearden et al., Phys. Rev. Lett. **88**, 202 301 (2002)
45. F. Aversa et al., Nucl. Phys. B **327**, 105 (1989); B. Jager et al., Phys. Rev. D **67**, 054 005 (2003); W. Vogelsang, private communication (NLO spectra have been computed with CTEQ6 PDFs, KKP FFs, and scales set to the hadron $p_{\mathrm{T}}$).
46. N. Hammon, A. Dumitru, H. Stoecker, W. Greiner, Phys. Rev. C **57**, 3292 (1998)

47. S.A. Bass, B. Muller, D.K. Srivastava, Phys. Rev. Lett. **90**, 082 301 (2003)
48. T. Renk, S.A. Bass, D.K. Srivastava, nucl-th/0505059
49. J. Berges, S. Borsanyi, C. Wetterich, Phys. Rev. Lett. **93**, 142 002 (2004)
50. P. Arnold, J. Lenaghan, G.D. Moore, L.G. Yaffe, nucl-th/0409068
51. P.F. Kolb, R. Rapp, Phys. Rev. C **67**, 044 903 (2003)
52. PHENIX Collaboration, S.S. Adler et al., Phys. Rev. C **69**, 034 909 (2004)
53. STAR Collaboration, J. Adams et al., Phys. Rev. Lett. **92**, 112 301 (2004)
54. STAR Collaboration, H. Caines, J. Phys G **31**, S101 (2005); STAR Collaboration, O. Barannikova, nucl-ex/0408022 and private communication
55. PHOBOS Collaboration, B.B. Back et al., Phys. Rev. C **70**, 051 901(R) (2004)
56. PHENIX Collaboration, S.S. Adler et al., Phys. Rev. Lett. **91**, 072 301 (2003)
57. STAR Collaboration, J. Adams et al., Phys. Rev. Lett. **91**, 172 302 (2003)
58. PHENIX Collaboration, K. Adcox et al., Phys. Rev. Lett. **88**, 242 301 (2002); PHENIX Collaboration, S.S. Adler et al., Phys. Rev. Lett. **91**, 172 301 (2003)
59. R.J. Fries, J. Phys G **30**, S853 (2004) and refs. therein
60. L.E. Gordon, W. Vogelsang, Phys. Rev. D **48**, 3136 (1993); Phys. Rev. D **50**, 1901 (1994); W. Vogelsang, private communication; also P. Aurenche et al., Phys. Lett. B **140**, 87 (1984); Nucl. Phys. B **297**, 661 (1988)
61. S. Kretzer, H.L. Lai, F.I. Olness, W.K. Tung, Phys. Rev. D **69**, 114 005 (2004)
62. M. Gluck, E. Reya, A. Vogt, Phys. Rev. D **48**, 116 (1993) [Erratum-ibid. D **51**, 1427 (1995)]
63. J. Jalilian-Marian, K. Orginos, I. Sarcevic, Phys. Rev. C **63**, 041 901 (2001)
64. PHENIX Collaboration, S. Bathe, nucl-ex/0511042, Quark Matter'05, Budapest, August 2005
65. F. Arleo, hep-ph/0406291
66. S. Turbide, C. Gale, S. Jeon, G.D. Moore, Phys. Rev. C **72**, 014 906 (2005)
67. D. d'Enterria, J. Phys G **31**, S491 (2005)
68. B.G. Zakharov, JETP Lett. **80**, 1 (2004) [Pisma Zh. Eksp. Teor. Fiz. **80**, 3 (2004)]
69. P. Arnold, G.D. Moore, L.G. Yaffe, JHEP **0112**, 009 (2001)
70. C.T. Traxler, H. Vija, M.H. Thoma, Phys. Lett. B **346**, 329 (1995)
71. F. Gelis, H. Niemi, P.V. Ruuskanen, S.S. Rasanen, J. Phys G **30**, S1031 (2004)
72. S. Turbide, R. Rapp, C. Gale, Phys. Rev. C **69**, 014 903 (2004)
73. O. Kaczmarek, F. Karsch, F. Zantow, P. Petreczky, Phys. Rev. D **70**, 074 505 (2004)
74. R.J. Fries, B. Muller, D.K. Srivastava, Phys. Rev. Lett. **90**, 132 301 (2003)
75. R.J. Fries, B. Muller, D.K. Srivastava, nucl-th/0507018
76. C. Albajar et al. [UA1 Collaboration], Phys. Lett. B **209**, 397 (1988)
77. F. Arleo, hep-ph/0601075
78. J.-e. Alam, J.K. Nayak, P. Roy, A.K. Dutt-Mazumder, B. Sinha, nucl-th/0508043
79. PHENIX Collaboration, Y. Akiba, nucl-ex/0510008, Quark Matter'05, Budapest, August 2005
80. B. Muller, K. Rajagopal, Eur. Phys. J. C **43**, 15 (2005)
81. D. d'Enterria, D. Peressounko, in preparation
82. See e.g. C.Y. Wong, Introduction to high-energy heavy ion collisions (World Scientific, Singapore 1994). Note that the relation $s = 4\zeta(4)/\zeta(3)\rho \approx 3.6\rho$ commonly found in the literature refers to an ideal gas of bosons. For an ideal gas of quarks and gluons (with $N_{B,F}$ bosons and fermions), the effective number of degrees of freedom for $\rho$ ($g_{\rm eff} = N_B + 3/4 \cdot N_F$) and for $\epsilon$ ($g_{\rm eff} = N_B + 7/8 \cdot N_F$, which "propagate" to the entropy density via: $s = (\epsilon + P)/3$) are slightly different. Thus, the right expression is $s \approx 4\rho$.